

Orbital forcing controlling dry time carbonate precipitation temperature over landmass in the northern mid-latitude during last 50,000 years revealed from carbonate clumped isotope thermometry

Yogaraj Banerjee¹, S. Thamizharasan^{2,3} and Prosenjit Ghosh^{1,2,3,*}

¹Interdisciplinary Centre for Water Research, Indian Institute of Science, Bengaluru 560 012, India

²Centre for Earth Sciences, Indian Institute of Science, Bengaluru 560 012, India

³Divecha Centre for Climate Change, Indian Institute of Science, Bengaluru 560 012, India

Indian Summer Monsoon is an integrated component of the global climate system. The spatial movement of ITCZ at seasonal and orbital time scales is revealed in the ensemble of terrestrial and marine records covering the last 50,000 years. We deduced an evolutionary shift in the precipitation pattern near western North America, Mediterranean and South East Asia based on the estimated water isotopic composition from the $\delta^{18}\text{O}_{\text{carbonate}}$ and Δ_{47} thermometer. Record revealed three stages of climate transition: mid-Holocene optima, Younger Dryas and Last glacial maxima. Estimated mean arid air temperature was 9–21°C and 12–35°C during the glacial and interglacial periods respectively. The June summer solar insolation at 65°N is captured in the temperature record linked with ice volume, atmospheric CO₂ levels and sea surface temperature; factors influencing the monsoon precipitation near mid-latitude region worldwide.

Keywords: Clumped isotopes, monsoon, orbital forcing.

Introduction

ORBITAL forcing is an important parameter known to regulate the redistribution of incoming solar radiation in the region of mid-latitudes over the Northern Hemisphere. The changes in orbital parameter modify the total amount of solar radiation reaching the mid-latitude region of the Earth by up to 25%, altering the zonal average temperature. The process imparts a shift in the potential gradient affecting the hydrological circulation. Both proxy and model-based studies have demonstrated the variation in the intensity of monsoon precipitation controlled by the orbital forcing^{1–3}. The response to the hydrological cycle due to a shift in the orbital parameter

varies within the mid-latitude zone of Northern Hemispheres. Here we have highlighted the variability of northern hemispheric temperature due to orbital forcing and resolved its effect on the freshwater availability due to the shift in the hydrological circulation. We used clumped isotope derived temperature estimates from well-preserved carbonate fossils and palaeo-archives originating for our study. The carbonate deposits considered here are mostly natural precipitate formed during the dry time because of conducive environmental condition promoting carbonate saturation^{4–7}. Thus temperature deduced here represents the average dry time temperature during glacial and interglacial period. Records of similar kind have been used by several workers for delineating the control mechanism of climatic oscillation due to a shift in the orbital parameter^{8–14}. The list of archives probed in this study includes: palaeosol carbonates^{4,15,16}, stromatolite^{17,18}, speleothems¹⁹ mollusc shells^{20,21}, lacustrine carbonate^{22,23} and subglacial carbonate²⁴. The sampling locations are displayed in Figure 1 and compartmentalized into three major sectors, namely Western North America, Mediterranean and South–East Asia.

The technique of carbonate clumped isotope is new and its reliability in deducing the past temperature within the uncertainty of $\pm 2^\circ\text{C}$ (refs 25, 26) is validated with multiple studies, thereby providing a unique tool to understand the temperature variability due to orbital forcing. The response of temperature change on the tropical hydroclimate was further used for derivation of $\delta^{18}\text{O}$ of water at the depositional environment²¹ and can be linked with the results obtained from the general circulation modelling experiments^{3,27}.

Orbital forcing and seasonal dry period temperature oscillation

Over the last one million year, earth's climate experienced frequent glacial/interglacial cycles, comprising

*For correspondence. (e-mail: pghosh@iisc.ac.in)

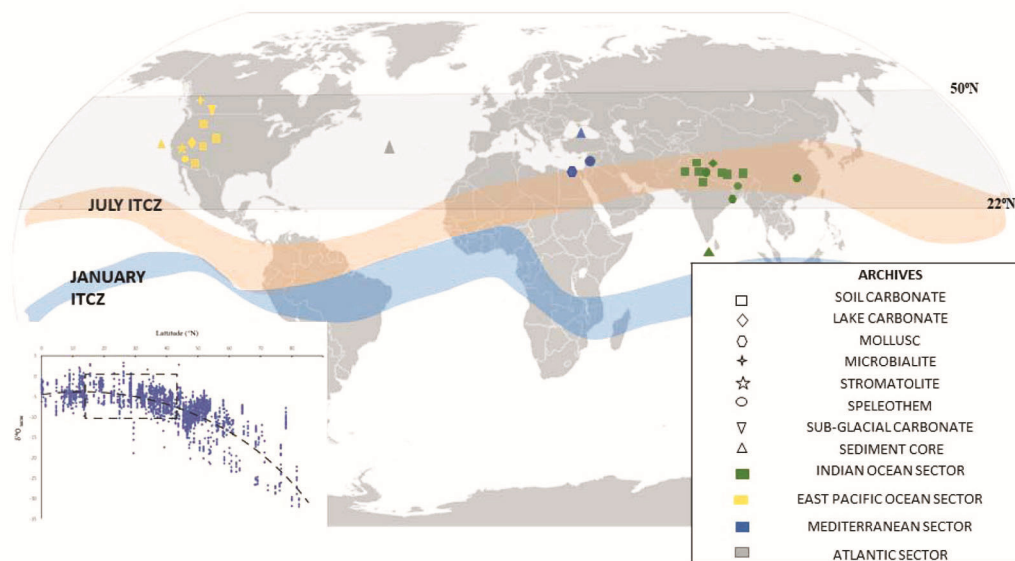


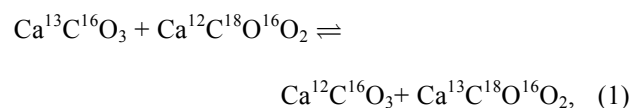
Figure 1. Location map of both terrestrial and marine carbonates used for this study. The location map shows different sites from continental archives documenting record of temperature change using clumped isotope analysis of soil carbonate, lacustrine carbonate^{4,15,16}, mollusc growth bands^{20,21}, microbialite¹⁷, freshwater stromatolite¹⁸, speleothem¹⁹ and sub-glacial carbonate²⁴. Temperature estimates from the TEX_{86} of Mawmluh speleothem³⁸ as well as Alkenone unsaturation index of a marine sediment core from Pacific⁶⁴, Atlantic⁴⁰ and Mediterranean⁴¹ and Mg/Ca from planktonic foraminifera from Equatorial Indian Ocean⁴² were collated in this study. Inset shows near-constant $\delta^{18}\text{O}$ in precipitation between 15°N and 40°N latitude collected at several sites scattered over the northern hemisphere (Asia, Europe and North America) based on GNIP dataset (<https://www.iaea.org/services/networks/gnip>).

41–100 kyr periodicities, established based on the high-resolution analysis of ice cores and marine sedimentary archives^{28,29}. An intense shift in the climate system during the period of the last three interglacial stages is perhaps most well documented in the marine isotope stages, where temperature estimates match with the $\delta^{18}\text{O}$ and CO_2 concentration measured in the trapped air packet present in the ice core record from the Antarctica region (Figure 2a)^{30,31}. The orbital factor of eccentricity and precession were held responsible in modulating the incoming solar radiation by ~10% due to the variation in the orbital geometry, the consequence of this on the average dry time temperature in a year for the northern hemisphere and its effects on the northern hemispheric water circulation or convective activity is documented in the present study. Here, we present a comprehensive record showing estimated dry time air temperature oscillation from western North America, Mediterranean and South East Asia using terrestrial carbonate clumped isotope, TEX_{86} records and compared it with sea surface temperature derived from the marine archives.

Carbonate clumped isotope thermometry

During the last decade, conventional oxygen isotope thermometry is replaced by more robust multi-substituted isotope-based thermometry²⁵. The major drawback of $\delta^{18}\text{O}$ based thermometry was phase dependency, where independent knowledge of water composition is rarely

deduced with confidence. This was circumvented in a few cases where diagenetic transformation was minimal and pore water fluids trapped in the sediments interspaced can be extracted for isotopic ratio determination³². The introduction of clumped isotope-based temperature estimation²⁵ addressed this problem by its virtue of being a lattice vibrational thermometer. Hence, using clumped isotopes one can derive the exact palaeotemperatures without any additional knowledge about water composition. It is based on the homogeneous isotope exchange equilibria (1) between different species of carbonate molecules (isotopologues), which results in a preferred bonding of heavy isotopes (^{13}C – ^{18}O) in carbonate isotopologues at varying temperatures^{25,33}.



The equilibrium constant K_{eq} depends on the temperature in such a way that the abundance of multiply substituted isotopologues increases with a decrease in the precipitation or crystallization temperatures. Thermodynamic driving forces lead to a higher-than-stochastic value for K_{eq} , i.e. $K_{\text{eq}} \cong 1$ at very high temperature. Lowering of temperature shifts reaction (1) towards the right with a sensitivity of about $-0.000003/\text{K}$ (refs 34, 35). Thus, the abundance of mass 47 isotopologues of CO_2 containing heavy isotopes of oxygen (O^{18}) and carbon (C^{13}) is purely

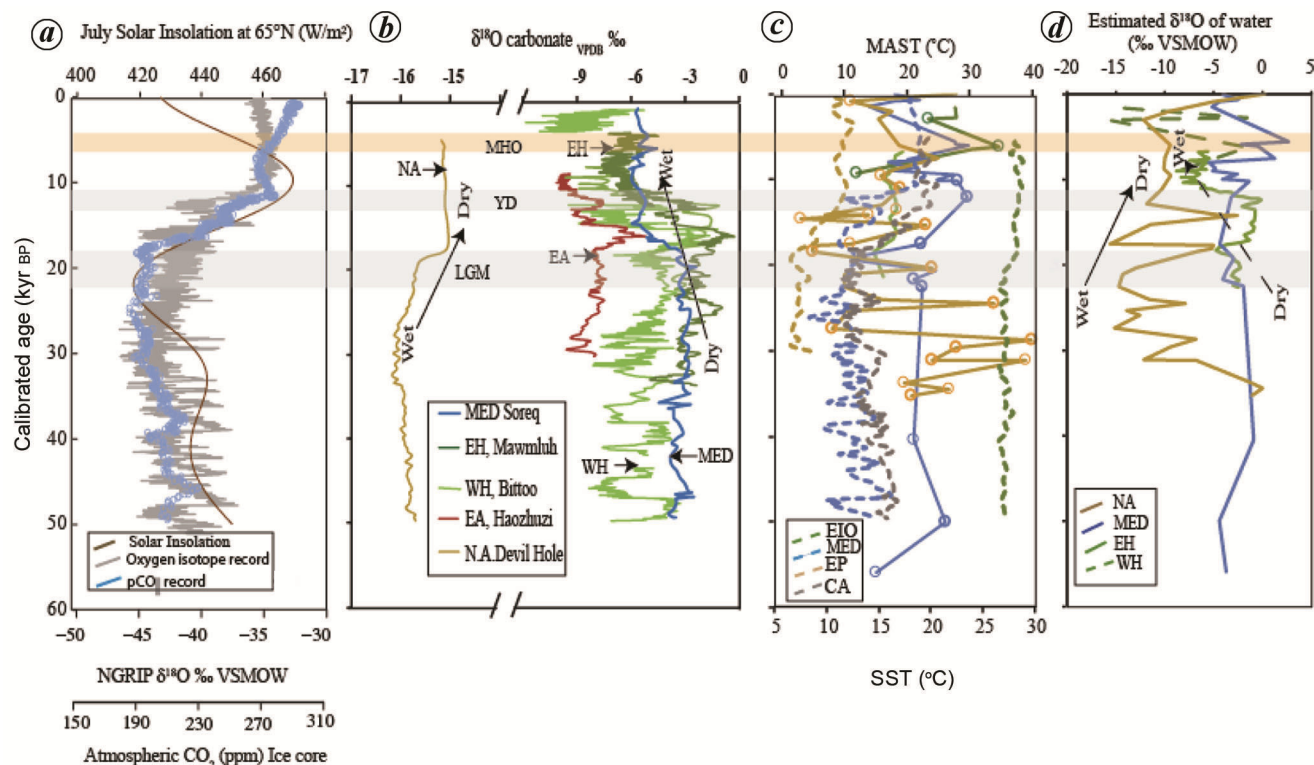


Figure 2. Glacial and interglacial variation of terrestrial temperature and oxygen isotopic composition of water during glacial–interglacial time periods over the northern mid-latitude. *a*, Temporal variation of solar insolation flux at 65°N (ref. 52) plotted along with $\delta^{18}\text{O}$ of water from NGRIP ice core⁵⁴ and atmospheric $p\text{CO}_2$ for past ~50 kyr BP (ref. 65). *b*, Variations in the $\delta^{18}\text{O}_{\text{carb}}$ composition of Speleothem archives for the past ~50 kyr BP distributed over the northern mid-latitudes, i.e. from western North America (NA), Mediterranean (MED), western Himalayas (WH), eastern Himalayas (EH) and south-east Asia (EA) studied by researchers^{19,66–70}. *c*, Mean atmospheric summertime temperature (MAST) and sea surface temperature (SST) during glacial–interglacial interval was established using Δ_{47} ARF (compilation of data in the present study), TEX_{86} of terrestrial carbonate³⁸ and Alkenone unsaturation index of marine sediment organic matter^{39,40–42}. The standard error (SE) for the measurement of clumped isotope temperature is 2°C. *d*, Variations in the $\delta^{18}\text{O}_{\text{water}}$ composition estimated from Δ_{47} based temperature and $\delta^{18}\text{O}_{\text{carb}}$ information compiled in this study, using the equilibrium relationship of precipitated calcite and oxygen isotopic composition of water by Kim and O’Neil⁴³.

temperature dependent in natural setup. Similarly, for carbonate, the CO_2 produced from the acid digestion of carbonate minerals was found proportional to the abundance of $^{13}\text{C}^{18}\text{O}^{16}\text{O}_2$ in the mineral. The clumped isotope thermometry (Δ_{47}) denotes the excess or deficit of isotopologue 47 in the sample CO_2 relative to the amount expected if the isotopologue 47 in CO_2 gas attains the stochastic distribution³⁵. Δ_{47} is defined by the equation

$$\Delta_{47} = \left\{ \left(\frac{R_{47}}{R_{47}^*} - 1 \right) - \left(\frac{R_{46}}{R_{46}^*} - 1 \right) - \left(\frac{R_{45}}{R_{45}^*} - 1 \right) \right\} \times 1000 \text{ (‰)}, \quad (2)$$

where R_{47} , R_{46} , R_{45} are abundance ratios of masses 47, 46 and 45 relative to mass 44. R_{45}^* , R_{46}^* , R_{47}^* are the corresponding ratios measured in the sample CO_2 once it attains stochastic distribution. These are calculated using the equations

$$\begin{aligned} R_{45}^* &= R^{13} + 2 \times R^{17}, \\ R_{46}^* &= 2 \times R^{18} + 2 \times R^{13} \times R^{17} + (R^{17})^2, \\ R_{47}^* &= 2 \times R^{13} \times R^{18} + 2 \times R^{17} \times R^{18} + R^{13} \times (R^{17})^2, \end{aligned}$$

where R^{13} , R^{17} and R^{18} are the abundance ratios of $^{13}\text{C}/^{12}\text{C}$, $^{17}\text{O}/^{16}\text{O}$ and $^{18}\text{O}/^{16}\text{O}$ for the sample CO_2 . R^{13} and R^{18} are obtained measuring the $\delta^{13}\text{C}_{\text{PDB}}$ and $\delta^{18}\text{O}_{\text{VSMOW}}$ values of the sample CO_2 , whereas R^{17} is calculated from R^{18} by assuming $R^{17} = 0.528 \times R^{18}$, holds good for mass-dependent fractionation.

Several equations are available for deriving temperature from Δ_{47} data on carbonates. Different authors have provided varying slope and intercept values of a linear equation to define the temperature calibration³⁶. Although, since inception 47 data are defined based on the deviation of sample CO_2 from random or stochastic CO_2 (ref. 25), recent literature introduced the concept of rigorous calibration based on equilibrated CO_2 at different temperatures, also known as Δ_{47} in CDES scale³⁷. Table 1 contains a list of data archives with publication details used in the present study (Figure 1). Also displayed are a kind of sample and the empirical equation used for the temperature deduction. Besides clumped isotope-based temperature data, alkenone-based temperature deduced from TEX_{86} for the Mawmluh speleothem was also listed³⁸ for comprehensive documentation of temperature shift from marine sediment core retrieved from the

Table 1. Latitudinal location, derived temperature range, age estimates and the equation used for the samples used in this study

Archive	Reference	Latitudinal range	Temperature range	Calibrated age range (kyr BP)	Equation for temperature
Clumped isotope thermometry (Δ_{37})					
Soil carbonate	8	27°11.841–38°49.048N	17.8°–38.5°C	0.640–21.160	[1]
	16	41.89°–44.21°N	17.6°–36.8°C	Hol.–Late Pleist.	[2]
	15	46.31348–46.77343°N	22°–5°C	8–27.3	[3]
Lake carbonate	22	36.30214°–39.753265°N	9.6°–22.7°C	Modem	[1]
	23	29.55814°–31.58836°N	9°–31°C	Modem	[3, 4]
Mollusc	20	31°–33°N	18.6°–29.9°C	Modem – 48.5	[3]
	21	22°N	21°–38°C	2.765	[2]
Microbialite	17	48°–50°N	11.2°–24.1°C	Modem – 9.5	[2]
Stromatolite	18	38.5°N	14.9°–33.6°C	Modem – 35.2	[2]
Speleothem	19	31.75545°N	19°–33.6°C	0.03–56	[1]
Sub-glacial carbonate	24	42.7°N	3°–15°C	Modem – 18.46	[5]
TEX ₈₆					
Speleothem	38	25.26°N	14.6°–19.4°C	6.75–21.37	[6]
Alkenone unsaturation index					
Pacific Ocean Marine sediment	39	42.26200°N	6.5°–6.5°C	Modem – 30.1	[7]
Atlantic Ocean Marine sediment	40	42.00°N	12.2°–20.6°C	5–50.03	[7]
Mediterranean Marine sediment	41	36.0317°N	8.4°–19.4°C	Present – 50.2	[8]
Mg/Ca ratio of <i>Globigerinoides ruber</i>					
Equatorial Indian Ocean Marine sediment	42	02.667°N	26.5°–28.9°C	Present – 49.7	[9]

Equation for temperature derived from different proxies

[1] Ref. 25: $\Delta_{47} = (0.0592 \times 10^6)/T^2 - 0.02$. [2] Ref. 37: $\Delta_{47} = (0.0636 \pm 0.00479 \times 10^6)/T^2 - (0.0047 \pm 0.0520)$.

[3] Ref. 71: $\Delta_{47} = (0.0526 \pm 0.0025 \times 10^6)/T^2 - (0.0520 \pm 0.0284)$. [4] Ref. 72: $\Delta_{47} = (0.0362 \times 10^6)/T^2 - (0.314)$.

[5] Ref. 73: $\Delta_{47} = (0.0417 \pm 0.0013 \times 10^6)/T^2 - (0.136 \pm 0.014)$. [6] Ref. 74: MAAT (°C) = $-7.4 \times (33.3 \times \text{TEX}_{86})$.

[7] Ref. 75: $U_{37}^k = (0.034 \times T) + 0.039$. [8] Ref. 76: $U_{37}^{kr} = (0.033 \times T) + 0.44$.

[9] Ref. 77: Mg/Ca = $0.38 \exp 0.09 [\text{SST} - 0.61 (\text{core depth km})]$.

Pacific³⁹, Atlantic⁴⁰, Mediterranean⁴¹ and Equatorial Indian Ocean⁴². The knowledge of the temperature of carbonate deposition allows estimation of water isotopic composition using the concept of equilibrium precipitation⁴³, where rainout process and accompanied Rayleigh fractionation are responsible for the variation of isotopic signature across the latitudes⁴⁴. It is known as the latitudinal effect of stable isotopes in precipitation, which defines a systematic polynomial shift in isotopic ratios in precipitation with latitudinal coordinates (Figure 1 inset). However, the observed variation in the isotopic composition of precipitation in the region of the mid-latitudes was minimal^{45,46}. This is mainly due to masking of other factors like convective activity in the Hadley cell and nature of moisture transport in the continental interiors⁴⁷. Therefore, data from all the sites covering a zone of mid-latitude can be binned to address the variability of convection process through time and space. The procedure of estimation of water isotopic composition involves temperature estimation using Δ_{47} , whereas $\delta^{18}\text{O}$ of carbonate measured during the analysis was used as the input variable in the empirical relationship⁴³ for the derivation of water isotopic composition. For example, the $\delta^{18}\text{O}$ of pe-

dogenic carbonate precipitated from the water in the terrestrial region is controlled by the land air temperature and composition of soil water. The $\delta^{18}\text{O}$ of soil water becomes lighter because of excess precipitation, whereas intense evaporation during drier condition causes enrichment in the $\delta^{18}\text{O}$ values.

Migration of ITCZ during glacial–interglacial cycles

Intertropical Convergence Zone (ITCZ) is a region of low-pressure in the mid-latitude, where moisture-laden jets of air converge at tropics depending on the apparent distribution of solar heating at a seasonal time interval. The position of the ITCZ can shift seasonally and also in longer timescale and is controlled by the latitudinal distribution of the solar insolation^{9,27,48,49}. In the long term glacial–interglacial time scale, apart from the North Atlantic glaciation and the Atlantic meridional overturning circulation (AMOC), precession cycle is one of the key factors that governs the migration of ITCZ⁵⁰. It is designated as a zone of convergence of the north-easterly and south-easterly trade winds. The region in the northern

hemisphere receives the maximum amount of precipitation or freshwater supply during the summer. The shift in terms of the position of ITCZ is of research interest for the climatologists over the last few decades^{48,51}. To understand the influence of orbital forcing on ITCZ migration and precipitation over the Northern Hemisphere landmass for the last 50,000 years, we have compiled the data on isotope derived temperature estimates from terrestrial carbonate archives which are spatially distributed across the mid-latitude region. These datasets registered a temporal shift in the July solar insolation flux at 65°N coinciding with the prominent precession periodicity of ~21 kyr (ref. 52; Figure 2a). The knowledge of the variability of solar insolation across the mid-latitude belt of the Northern Hemisphere can be compared with the glacial–interglacial temperature (Figure 2a). It shows a gradual drop in the solar insolation value from MIS 3 (~450 Wm⁻²) to the last glacial maxima (~418 Wm⁻²), which resulted in a shift in the onset of continental glaciation in the polar region of the northern hemisphere. This was followed by a ~40 Wm⁻² rise in the solar insolation during post LGM and early Holocene period which caused ~120 m rise of mean sea level as a consequence of melting of glacial ice sheets⁵³. From early Holocene onwards, the solar insolation steadily reduces from ~470 Wm⁻² to the present-day value of ~427 Wm⁻² (1950 AD). We have further compared the insolation variability with the $\delta^{18}\text{O}$ record from the Northern Greenland ice core (GRIP)⁵⁴. The $\delta^{18}\text{O}$ of the NGRIP ice core depends on the latitudinal temperature gradient and the moisture-holding capacity of air packet found in the poleward moving air masses⁵⁵. Modelling of temperature profile along the GRIP data shows an average drop in oxygen isotopic ratio by 5‰ during LGM compared to the MIS 3 owing to the ~20°C reduction in the regional temperature near northern Greenland and the consequent drop in the moisture-holding capacity of the air parcels⁵⁶. In contrast, an 11‰ enrichment during the early Holocene was recorded compared to the average value observed during LGM. This can be explained by ~25°C rise in the northern Greenland temperature during the early Holocene⁵⁷.

Temperature variability

Compilation of the data of the clumped isotope (Δ_{47}) temperatures (Figure 2b) and the deduced $\delta^{18}\text{O}_{\text{water}}$ (Figure 2c) from the mid-latitude terrestrial carbonates showed a range in temperature values, i.e. from ~35°C to 9°C, and the corresponding range in water isotopic composition was 2.5‰ to -15‰ respectively, over the last 50,000 years that includes spatial variability along with several episodes of warming and cooling intervals. The spatial variability of carbonate precipitation temperature showed a significant contrast across the mid-latitude

region; while palaeosols from Northern American flood plain and South–East Asian archives recorded a bigger shift in temperature values (i.e. 9–19°C for western North American and 17–35°C in South East Asia). The Mediterranean terrestrial carbonate archives registered a smaller shift (i.e. 24–30°C) in temperature values. However, the record from South East Asia comprises regions with varying elevation, including temperature information derived from other proxies like TEX₈₆ in speleothem and clumped isotopes in mollusc and palaeosols. During colder climate such as Last Glacial Maxima and Younger Dryas, the terrestrial dry time air temperatures over western North America were ~10–23°C and ~15°C respectively. Similarly, for the Mediterranean ~21°C and ~25°C were recorded during Last Glacial Maxima and Younger Dryas. Likewise, South East Asia registered ~15°C and ~16°C during Last Glacial Maxima and Younger Dryas. However, temperature variability during MHO was minimal based on the continental record. This temperature contrast at different time interval allowed the establishment of varied land–sea potential gradient influencing hydrological cycle.

Land sea temperature contrast

Land sea temperature contrast was significantly higher during warmer periods in the western North American region (Figure 2c); however, the difference was lower in the Mediterranean and South–East Asian sectors. This was the primary driver for the advective process to actuate, which promoted the transfer of low-density air parcel from the oceanic region to the continental settings (Figure 3a–c). During the colder period, land–sea temperature contrast was lower than the Holocene in all the regions. Sea temperatures were rather constant throughout the section. However, the land temperature was oscillating owing to other factors like the nature of archives¹⁵.

Water isotopic composition variability

The water isotopic values estimated over the mid-latitude region suggest dry and wetter condition. The sedimentary archive documenting LGM from western North America showed $\delta^{18}\text{O}$ of water as -15‰, while the Mediterranean and South East Asia carbonate archives recorded the isotopic composition of -3‰ and -1.5‰ respectively (Figure 2d). The enriched $\delta^{18}\text{O}_{\text{water}}$ values in this time interval suggest more evaporation at a relatively higher temperature during the dry time or less transport of moisture from the ocean due to a reduction in the advective activities. Thus, we speculate that the lowering of northern hemisphere temperature during LGM caused southward migration of the ITCZ. The migration of ITCZ in the southern hemisphere is also revealed from the isotopic record in the marine sedimentary archives^{58,59}.

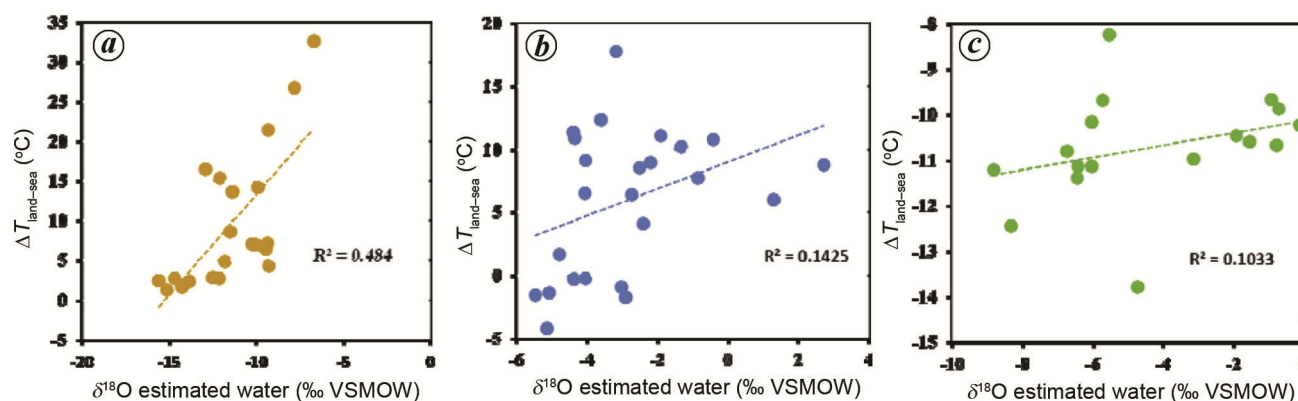


Figure 3. Relationships between land–sea temperature contrast (ΔT) and $\delta^{18}\text{O}$ composition of the estimated precipitation water for (a) Western North America, (b) the Mediterranean and (c) South–East Asia continents. a, For western North America compiled clumped isotope temperature data from terrestrial archives (except Hough *et al.*¹⁶) and Alkenone unsaturation index based SST of eastern Pacific were used. b, Compiled clumped isotope temperature data from terrestrial archives and Alkenone unsaturation index based SST were used to obtain ΔT for the Mediterranean. c, For the South East Asia TEX₈₆ temperature data from terrestrial archives and Mg/Ca based SST of equatorial Indian Ocean were used to get the land–sea temperature contrast.

East-west climatological contrast

Arid climate prevailed during Holocene in Western North America, however, the Mediterranean and South-East Asian sectors witnessed warming and wetter climate during Holocene. Thus, the ITCZ moves towards the northern hemisphere during the period of a warmer climate over the Asian region and receded southward over the western North American continent. We observed an increment in $\delta^{18}\text{O}$ of water during the period of mid-Holocene optima (MHO) suggesting drier condition over the terrestrial mid latitudinal environment. This is consistent with the argument of a southward shift of ITCZ in the Pacific during Holocene⁶⁰ and greening of Sahara during MHO⁶¹ with apparent migration of ITCZ towards western northern hemisphere⁶². A drop in precipitation amount during MHO in western North America was attributed to lesser transport of moisture from the Pacific to the continental interior as a consequence of lower temperature gradient between Pacific and Continental interior (Figure 2c). This is consistent with the GCM model prediction showing a drier condition during MHO over the regions of the United States⁶². Wetter condition over South Asia mostly the Himalayan region during mid-Holocene optima was due to the strengthening of South-East Asian Monsoon⁶³.

Conclusion

We have presented the first compilation of temperature data from terrestrial archives covering the region of northern hemisphere mid-latitude region. This allowed removal of temperature effect in the stable oxygen isotopic composition of terrestrial carbonates of varied origin.

The scatter in the temperature record is mainly due to the diverse nature of the samples and mode of occur-

rences. Our observation showed heavier isotopic value during Holocene from the region of western North America, which is in contrast to the lighter isotopic composition noted in the record from the Mediterranean and South-East Asian sectors. This observation is further validated with the air–sea temperature contrast documented from both marine and terrestrial archives. This has an important implication in the era of global pCO₂ rise, where the warming is responsible for the drastic modification of the modern climate in the region of mid-latitudes.

1. Tiwari, M., Ramesh, R., Somayajulu, B. L. K., Jull, A. T. and Burr, G. S., Paleomonsoon precipitation deduced from a sediment core from the equatorial Indian Ocean. *Geo-Marine Lett.*, 2006, **26**(1), 23–30.
2. Ramesh, R., Tiwari, M., Chakraborty, S., Managave, S. R., Yadava, M. G. and Sinha, D. K., Retrieval of south Asian monsoon variation during the Holocene from natural climate archives. *Curr. Sci.*, 2010, **99**(12), 1770–1786.
3. Jalihal, C., Bosmans, J. H. C., Srinivasan, J. and Chakraborty, A., The response of tropical precipitation to Earth's precession: the role of energy fluxes and vertical stability. *Climate Past*, 2019, **15**(2), 449–462.
4. Quade, J., Eiler, J., Daeron, M. and Achyuthan, H., The clumped isotope geothermometer in soil and paleosol carbonate. *Geochim. Cosmochim. Acta*, 2013, **105**, 92–107.
5. Kaźmierczak, J., Fenchel, T., Kűhl, M., Kempe, S., Kremer, B., Łącka, B. and Małkowski, K., CaCO₃ precipitation in multilayered cyanobacterial mats: clues to explain the alternation of micrite and sparite layers in calcareous stromatolites. *Life*, 2015, **5**(1), 744–769.
6. Leng, M. J. and Lewis, J. P., Oxygen isotopes in Molluscan shell: applications in environmental archaeology. *Environ. Archaeol.*, 2016, **21**(3), 295–306.
7. Ronay, E. R., Breitenbach, S. F. and Oster, J. L., Sensitivity of speleothem records in the Indian Summer Monsoon region to dry season infiltration. *Scientific Rep.*, 2019, **9**(1), 5091.
8. Kemp, D. B., Van Manen, S. M., Pollitt, D. A. and Burgess, P. M., Investigating the preservation of orbital forcing in peritidal carbonates. *Sedimentology*, 2016, **63**(6), 1701–1718.
9. Zhang, S. *et al.*, Orbital forcing of climate 1.4 billion years ago. *Proc. Natl. Acad. Sci.*, 2015, **112**(12), E1406–E1413.

10. Clemens, S. C., Prell, W. L. and Sun, Y., Orbital-scale timing and mechanisms driving Late Pleistocene Indo-Asian summer monsoons: reinterpreting cave speleothem $\delta^{18}\text{O}$. *Paleoceanography*, 2010, **25**(4).
11. Sano, Y. *et al.*, Past daily light cycle recorded in the strontium/calcium ratios of giant clam shells. *Nature Commun.*, 2012, **3**, 761.
12. Gizzi, F. *et al.*, Shell properties of commercial clam *Chamelea gallina* are influenced by temperature and solar radiation along a wide latitudinal gradient. *Scientific Rep.*, 2016, **6**, 36420.
13. DeBoer, P. L. and Smith, D. G. (eds), *Orbital Forcing and Cyclic Sequences*, John Wiley, 2009, vol. 38.
14. Van Vugt, N., Langereis, C. G. and Hilgen, F. J., Orbital forcing in Pliocene–Pleistocene Mediterranean lacustrine deposits: dominant expression of eccentricity versus precession. *Palaeogeogr., Palaeoclimatol., Palaeoecol.*, 2001, **172**(3–4), 193–205.
15. Lechler, A. R., Huntington, K. W., Breecker, D. O., Sweeney, M. R. and Schauer, A. J., Loess–paleosol carbonate clumped isotope record of late Pleistocene–Holocene climate change in the Palouse region, Washington State, USA. *Quatern. Res.*, 2018, **90**(2), 331–347.
16. Hough, B. G., Fan, M. and Passey, B. H., Calibration of the clumped isotope geothermometer in soil carbonate in Wyoming and Nebraska, USA: implications for paleoelevation and paleoclimate reconstruction. *Earth Planet. Sci. Lett.*, 2014, **391**, 110–120.
17. Petryshyn, V. A., Lim, D., Laval, B. L., Brady, A., Slater, G. and Tripathi, A. K., Reconstruction of limnology and microbialite formation conditions from carbonate clumped isotope thermometry. *Geobiology*, 2015, **13**(1), 53–67.
18. Petryshyn, V. A., Rivera, M. J., Agić, H., Frantz, C. M., Corsetti, F. A. and Tripathi, A. E., Stromatolites in Walker Lake (Nevada, Great Basin, USA) record climate and lake level changes ~35,000 years ago. *Palaeogeogr., Palaeoclimatol., Palaeoecol.*, 2016, **451**, 140–151.
19. Affek, H. P., Guo, W., Daeron, M. and Eiler, J. M., ‘Clumped isotopes’ in speleothem carbonate and atmospheric CO_2 – is there a kinetic isotope effect? *Geochim. Cosmochim. Acta*, 2008, **72**(12), A6–A6.
20. Zaarur, S., Affek, H. P. and Stein, M., Last glacial–Holocene temperatures and hydrology of the Sea of Galilee and Hula Valley from clumped isotopes in Melanopsis shells. *Geochim. Cosmochim. Acta*, 2016, **179**, 142–155.
21. Banerjee, Y., Ghosh, P., Bhushan, R. and Rahul, P., Strong sea forcing and warmer winter during solar minima ~2765 year BP recorded in the growth bands of *Crassostrea* sp. from the confluence of river Ganges, Eastern India. *Quat. Int.*, 2018, **479**, 48–57.
22. Huntington, K. W., Wernicke, B. P. and Eiler, J. M., Influence of climate change and uplift on Colorado Plateau paleotemperatures from carbonate clumped isotope thermometry. *Tectonics*, 2010, **29**(3).
23. Huntington, K. W., Saylor, J., Quade, J. and Hudson, A. M., High late Miocene–Pliocene elevation of the Zhada Basin, southwestern Tibetan Plateau, from carbonate clumped isotope thermometry. *Bulletin*, 2015, **127**(1–2), 181–199.
24. Hudson, A. M. *et al.*, Stable C, O and clumped isotope systematics and ^{14}C geochronology of carbonates from the Quaternary Chewau can closed-basin lake system, Great Basin, USA: implications for paleoenvironmental reconstructions using carbonates. *Geochim. Cosmochim. Acta*, 2017, **212**, 274–302.
25. Ghosh, P. *et al.*, ^{13}C – ^{18}O bonds in carbonate minerals: a new kind of paleothermometer. *Geochim. Cosmochim. Acta*, 2006, **70**(6), 1439–1456.
26. Eiler, J. M., Paleoclimate reconstruction using carbonate clumped isotope thermometry. *Quat. Sci. Rev.*, 2011, **30**(25–26), 3575–3588.
27. Clement, A. C., Hall, A. and Broccoli, A. J., The importance of precessional signals in the tropical climate. *Climate Dyn.*, 2004, **22**(4), 327–341.
28. Waelbroeck, C., Jouzel, J., Labeyrie, L., Lorius, C., Labracherie, M., Stiévenard, M. and Barkov, N. I., A comparison of the Vostok ice deuterium record and series from Southern Ocean core MD 88-770 over the last two glacial–interglacial cycles. *Climate Dyn.*, 1995, **12**(2), 113–123.
29. Augustin, L. *et al.*, Eight glacial cycles from an Antarctic ice core. *Nature*, 2004, **429**, 623–628.
30. Neftel, A., Oeschger, H., Staffelbach, T. and Stauffer, B., CO_2 record in the Byrd ice core 50,000–5000 years BP. *Nature*, 1988, **331**(6157), 609.
31. Yiou, P. *et al.*, High-frequency paleovariability in climate and CO_2 levels from Vostok ice core records. *J. Geophys. Res.: Solid Earth*, 1991, **96**(B12), 20365–20378.
32. Adkins, J. F., McIntyre, K. and Schrag, D. P., The salinity, temperature, and $\delta^{18}\text{O}$ of the glacial deep ocean. *Science*, 2002, **298**(5599), 1769–1773.
33. Wang, Z., Schauble, E. A. and Eiler, J. M., Equilibrium thermodynamics of multiply substituted isotopologues of molecular gases. *Geochim. Cosmochim. Acta*, 2004, **68**(23), 4779–4797.
34. Schauble, E. A., Ghosh, P. and Eiler, J. M., Preferential formation of ^{13}C – ^{18}O bonds in carbonate minerals, estimated using first-principles lattice dynamics. *Geochim. Cosmochim. Acta*, 2006, **70**(10), 2510–2529.
35. Eiler, J. M., ‘Clumped-isotope’ geochemistry – the study of naturally-occurring, multiply-substituted isotopologues. *Earth Planet. Sci. Lett.*, 2007, **262**(3–4), 309–327.
36. Spencer, C. and Kim, S. T., Carbonate clumped isotope paleothermometry: a review of recent advances in CO_2 gas evolution, purification, measurement and standardization techniques. *Geosci. J.*, 2015, **19**(2), 357–374.
37. Dennis, K. J., Affek, H. P., Passey, B. H., Schrag, D. P. and Eiler, J. M., Defining an absolute reference frame for ‘clumped’ isotope studies of CO_2 . *Geochim. Cosmochim. Acta*, 2011, **75**(22), 7117–7131.
38. Huguet, C. *et al.*, Temperature and monsoon tango in a tropical stalagmite: last glacial–interglacial climate dynamics. *Sci. Rep.*, 2018, **8**(1), 5386.
39. Prah, F. G., Piasis, N., Sparrow, M. A. and Sabin, A., Assessment of sea-surface temperature at 42°N in the California current over the last 30,000 years. *Paleoceanogr. Palaeoclimatol.*, 1995, **10**(4), 763–773.
40. Naafs, B. D. A., Heftler, J., Gruetzner, J. and Stein, R., Warming of surface waters in the mid-latitude North Atlantic during Heinrich events. *Paleoceanography*, 2013, **28**(1), 153–163.
41. Martrat, B., Grimalt, J. O., Shackleton, N. J., de Abreu, L., Hutterli, M. A. and Stocker, T. F., Four climate cycles of recurring deep and surface water destabilizations on the Iberian margin. *Science*, 2007, **317**(5837), 502–507.
42. Saraswat, R., Nigam, R., Weldeab, S., Mackensen, A. and Naidu, P. D., A first look at past sea surface temperatures in the equatorial Indian Ocean from Mg/Ca in foraminifera. *Geophys. Res. Lett.*, 2005, **32**(24).
43. Kim, S. T. and O’Neil, J. R., Equilibrium and nonequilibrium oxygen isotope effects in synthetic carbonates. *Geochim. Cosmochim. Acta*, 1997, **61**(16), 3461–3475.
44. Rozanski, K., Araguás-Araguás, L. and Gonfiantini, R., Isotopic patterns in modern global precipitation. *Climate Change Continental Isotopic Rec.*, 1993, 1–36.
45. Bowen, G. J. and Wilkinson, B., Spatial distribution of $\delta^{18}\text{O}$ in meteoric precipitation. *Geology*, 2002, **30**(4), 315–318.
46. Ghosh, P. *et al.*, Tracking the migration of the Indian continent using the carbonate clumped isotope technique on Phanerozoic soil carbonates. *Sci. Rep.*, 2016, **6**, 22187.
47. Gat, J. R., Klein, B., Kushnir, Y., Roether, W., Wernli, H., Yam, R. and Shemesh, A., Isotope composition of air moisture over the Mediterranean Sea: an index of the air–sea interaction pattern. *Tellus B: Chem. Phys. Meteorol.*, 2003, **55**(5), 953–965.
48. Broccoli, A. J., Dahl, K. A. and Stouffer, R. J., Response of the ITCZ to Northern Hemisphere cooling. *Geophys. Res. Lett.*, 2006, **33**(1).

49. Sloan, L. C. and Huber, M., Eocene oceanic responses to orbital forcing on precessional time scales. *Paleoceanogr. Paleoclimatol.*, 2001, **16**(1), 101–111.
50. Bond, G., Broecker, W., Johnsen, S., McManus, J., Labeyrie, L., Jouzel, J. and Bonani, G., Correlations between climate records from North Atlantic sediments and Greenland ice. *Nature*, 1993, **365**(6442), 143.
51. Haug, G. H., Hughen, K. A., Sigman, D. M., Peterson, L. C. and Röhl, U., Southward migration of the intertropical convergence zone through the Holocene. *Science*, 2001, **293**(5533), 1304–1308.
52. Berger, A. and Loutre, M. F., Insolation values for the climate of the last 10 million years. *Quat. Sci. Rev.*, 1991, **10**(4), 297–317.
53. Lambeck, K., Rouby, H., Purcell, A., Sun, Y. and Sambridge, M., Sea level and global ice volumes from the Last Glacial Maximum to the Holocene. *Proc. Natl. Acad. Sci.*, 2014, **111**(43), 15296–15303.
54. Andersen, K. K. *et al.*, High-resolution record of Northern Hemisphere climate extending into the last interglacial period. *Nature*, 2004, **431**(7005), 147.
55. Johnsen, S. J., Dansgaard, W. and White, J. W. C., The origin of Arctic precipitation under present and glacial conditions. *Tellus B: Chem. Phys. Meteorol.*, 1989, **41**(4), 452–468.
56. Johnsen, S. J., Dahl-Jensen, D., Dansgaard, W. and Gundestrup, N., Greenland palaeotemperatures derived from GRIP bore hole temperature and ice core isotope profiles. *Tellus B: Chem. Phys. Meteorol.*, 1995, **47**(5), 624–629.
57. Krinner, G. and Genthon, C., GCM simulations of the Last Glacial Maximum surface climate of Greenland and Antarctica. *Climate Dyn.*, 1998, **14**(10), 741–758.
58. Wang, Y. *et al.*, The Holocene Asian monsoon: links to solar changes and North Atlantic climate. *Science*, 2005, **308**(5723), 854–857.
59. Mukherjee, P., Sinha, N. and Chakraborty, S., Investigating the dynamical behavior of the Intertropical Convergence Zone since the last glacial maximum based on terrestrial and marine sedimentary records. *Quatern. Int.*, 2017, **443**, 49–57.
60. Sachs, J. P., Blois, J. L., McGee, T., Wolhowe, M., Haberle, S., Clark, G. and Atahan, P., Southward shift of the Pacific ITCZ during the Holocene. *Paleoceanogr., Paleoclimatol.*, 2018, **33**(12), 1383–1395.
61. Claussen, M. and Gayler, V., The greening of the Sahara during the mid-Holocene: results of an interactive atmosphere-biome model. *Global Ecol. Biogeography Lett.*, 1997, 369–377.
62. Shin, S. I., Sardeshmukh, P. D., Webb, R. S., Oglesby, R. J. and Barsugli, J. J., Understanding the mid-Holocene climate. *J. Climate*, 2006, **19**(12), 2801–2817.
63. Clift, P. D. and Plumb, R. A., *The Asian Monsoon: Causes, History and Effects*, Cambridge University Press, Cambridge, 2008, vol. 288.
64. Prah, F. G., Piasias, N., Sparrow, M. A. and Sabin, A., Assessment of sea-surface temperature at 42°N in the California current over the last 30,000 years. *Paleoceanography*, 1995, **10**(4), 763–773.
65. Bereiter, B. *et al.*, Revision of the EPICA Dome C CO₂ record from 800 to 600 kyr before present. *Geophys. Res. Lett.*, 2015, **42**(2), 542–549.
66. Landwehr *et al.*, The chronology for the $\delta^{18}\text{O}$ record from Devils Hole, Nevada, extended into the mid-Holocene. *US Geol. Surv. Open-File Rep.*, 2011, **1082**(5).
67. Berkelhammer, M., Sinha, A., Stott, L., Cheng, H., Pausata, F. S. and Yoshimura, K., An abrupt shift in the Indian monsoon 4000 years ago. *Geophys. Monogr. Ser.*, 2012, **198**, 75–87.
68. Dutt, S., Gupta, A. K., Clemens, S. C., Cheng, H., Singh, R. K., Kathayat, G. and Edwards, R. L., Abrupt changes in Indian summer monsoon strength during 33,800 to 5500 years BP. *Geophys. Res. Lett.*, 2015, **42**(13), 5526–5532.
69. Kathayat, G. *et al.*, Indian monsoon variability on millennial-orbital timescales. *Sci. Rep.*, 2016, **6**, 24374.
70. Zhang, H. *et al.*, Antarctic link with East Asian summer monsoon variability during the Heinrich Stadial–Bölling interstadial transition. *Earth Planet. Sci. Lett.*, 2016, **453**, 243–251.
71. Zaarur, S., Affek, H. P. and Brandon, M. T., A revised calibration of the clumped isotope thermometer. *Earth Planet. Sci. Lett.*, 2013, **382**, 47–57.
72. Eagle, R. A. *et al.*, The influence of temperature and seawater carbonate saturation state on ^{13}C – ^{18}O bond ordering in bivalve mollusks. *Biogeosciences*, 2013, **10**, 4591.
73. Kelson, J. R., Huntington, K. W., Schauer, A. J., Saenger, C. and Lechler, A. R., Toward a universal carbonate clumped isotope calibration: diverse synthesis and preparatory methods suggest a single temperature relationship. *Geochim. Cosmochim. Acta*, 2017, **197**, 104–131.
74. Blyth, A. J. and Schouten, S., Calibrating the glycerol dialkyl glycerol tetraether temperature signal in speleothems. *Geochim. Cosmochim. Acta*, 2013, **109**, 312–328.
75. Prah, F. G., Muehlhausen, L. A. and Zahnle, D. L., Further evaluation of long-chain alkenones as indicators of paleoceanographic conditions. *Geochim. Cosmochim. Acta*, 1988, **52**(9), 2303–2310.
76. Müller, P. J., Kirst, G., Ruhland, G., Von Storch, I. and Rosell-Melé, A., Calibration of the alkenone paleotemperature index U_{37K'} based on core-tops from the eastern South Atlantic and the global ocean (60°N–60°S). *Geochim. Cosmochim. Acta*, 1998, **62**(10), 1757–1772.
77. Dekens, P. S., Lea, D. W., Pak, D. K. and Spero, H. J., Core top calibration of Mg/Ca in tropical foraminifera: refining paleotemperature estimation. *Geochem., Geophys., Geosyst.*, 2002, **3**(4), 1–29.

ACKNOWLEDGEMENTS. Y.B. and P.G. thank the Ministry of Earth Sciences, Government of India (MoES/PAMC/H&C/41/2013-PC-II DT.17/7/18) and T.S. thanks Divecha Centre for Climate Change, Grantham Foundation for funding. We thank Mr R. Pandey of Hansraj College, Delhi University for helping in the initial data compilation as part of his summer internship project. We also thank the handling editors and two anonymous reviewers for their valuable suggestions in improving the quality of the manuscript. P.G. initiated the project. Y.B. and P.G. compiled the data and coordinated the work, P.G., Y.B. and T.S. designed the project and wrote the paper.

doi: 10.18520/cs/v119/i2/265-272